



ARTICLE

Alkaline Treatment of Straw for Composite Material Production and Its Impact on Water Vapor Adsorption Characteristics

Martin Böhm*, Miloš Jerman, Martin Keppert, Klára Kobetičová, Dana Koňáková, Milena Pavlíková and Robert Černý

Department of Materials Engineering and Chemistry, Faculty of Civil Engineering, Czech Technical University in Prague, Thákurova 7, Prague, 166 29, Czech Republic

*Corresponding Author: Martin Böhm. Email: martin.bohm@fsv.cvut.cz

Received: 04 August 2024 Accepted: 23 October 2024 Published: 20 February 2025

ABSTRACT

The effect of using 2% and 10% sodium hydroxide solution as surface treatment of rape straw on its water vapor adsorption properties is analyzed in the relative humidity (RH) range of 0% to 98%. Scanning electron microscopy (SEM), energy dispersive spectroscopy (EDS), and Fourier-transform infrared spectroscopy (FTIR) are used to investigate the morphological, chemical and structural changes of the treated straw surface. The mineral particles formed on the surface after the treatment are analyzed using X-ray diffraction (XRD). The application of sodium hydroxide solution results in the disruption of the straw surface. As the concentration of sodium hydroxide increases, the disruption of the straw surface increases, and the ability of the straw to adsorb water vapor also increases over the entire RH range. In addition to the surface disruption and chemical changes caused by the alkaline treatment, the differences in the equilibrium moisture content of treated and untreated rape straw can also be attributed to the formation of minerals on the straw surface, namely calcite for the 2% sodium hydroxide solution, and gaylussite and thermonatrite for the 10% solution.

KEYWORDS

Modification of straw surface; alkaline treatment; sorption mechanism; Guggenheim-Anderson-de Boer model (GAB)

1 Introduction

There are several approaches to reducing the negative environmental impact of the construction and operation of buildings. A promising and easy-to-apply approach is the use of renewable plant residues from local crops, which can be combined with a suitable organic binder to produce eco-friendly composites [1–3].

Globally, rapeseed (*Brassica napus* L.) is one of the most important oilseed crops, providing more than 15% of the world's vegetable oil supply [4], making it the third most important oilseed crop after soybean and palm [5]. Rape straw is mainly used for agricultural purposes as a by-product, or can be useful as a source for biofuel production [6,7]. In some cases, post-harvest rapeseed residues are even burned [8]. However, this lignocellulosic biomass can be utilized in a variety of applications, including the production of composites.



The cellulose content of rape straw is typically 40%–44%, with about 15%–16% lignin content [5]. Other authors report a similar composition of rape straw: 41% cellulose, 23.4% hemicellulose, 21.5% lignin, 6.8% extractives, and 5.8% ash [9], or in more detail according to the dry matter content of the rape straw (mean values and standard deviations in parentheses) 88.29% (± 0.21): ash content 1.97% (± 0.25), total protein content 2.09% (± 0.08), diethyl ether extractable substance represented 2.21% (± 0.98), hemicellulose 14.55% (± 0.34), acetyl groups 2.32% (± 0.29), cellulose 49.18% (± 0.42), acid insoluble lignin 17.65% (± 0.16), and acid soluble lignin 3.94% (± 0.19) [10].

When compared to other non-woody plants, rape straw's cellulose content is similar [11], but it is lower than that of softwoods [12], while its lignin content is comparable to that of hardwood cell walls. The structure of lignin is similar to that of angiosperm wood, with a low syringyl/guaiacyl ratio in the cell walls. This combination of properties has also sparked interest in its potential as a raw material for the pulp and paper industry [13]. The composition of rape straw hemicellulose is related to that of wood. Of the total 22.9%, it was found to consist of xylan (18.5%), galactan (2.2%), arabinan (1.0%), and mannan (1.2%) [14]. A comparison of the chemical composition of rape straw from various sources is summarized in Table 1.

Table 1: Percentage chemical composition of rape straw reported in the literature

Source	[5]	[15]	[1]	[16]	[13]	[17]	[18]
Cellulose	–	37.55	53.06	41.00	40–44	37.70	41.66
Hemicellulose	–	31.37	18.13	23.40	30–31	29.6 (Pentosans)	37.24
Holocellulose	58.51	–	–	–	–	–	–
Lignin	15.52	21.30	9.63	21.50	19–21	26.40	16.00
Extractives	17.16	–	–	6.80	0.2–0.4 (Silica)	–	1.63
Ash	8.80	6.02	0.79	5.80	2–3 (Inorganic)	0.05	3.46

One of the challenges in manufacturing composite materials from post-harvest residues is that their surface is often covered with a waxy layer that reduces the adhesion of the adhesive [19,20]. Various methods are available for treating the straw surface, including thermomechanical [21], chemical [21,22], or enzymatic treatment [23,24]. The surface of the straw can also be washed with hot or cold water [25], or alternatively, plasma treatment can modify its surface properties [25,26]. A new generation of physically assisted pretreatments (microwaves, ultrasound, pulsed electric fields, high-voltage electrical discharges, etc.) is also being developed [27].

Chemical treatment involves acidic or alkaline methods. Acidic treatments primarily remove hemicellulose and slightly increase cellulose crystallinity [28,29], while alkaline treatments are used to remove lignin and various uronic acid substitutions on hemicellulose. Sodium hydroxide (NaOH) is one of the most commonly used alkaline treatments for this purpose [30–32]. The principle of treatment with sodium hydroxide consists of delignification by breaking ester bonds that cross-link lignin and xylan [6]. Additionally, treatment with NaOH increases both porosity and the specific surface area of the material [6,33]. The nature of the particle surface strongly influences the contact angle and wettability of the adhesive, which is particularly important for water-based adhesives [25].

Relatively diluted NaOH solutions are commonly used to treat lignocellulosic particles, and this method has proven particularly effective in producing composite boards. The optimal concentration of NaOH for treating various natural raw materials remains an area of active research. Moreover, finding the right combination of straw treatment and adhesive mixture is equally important. Studies

have demonstrated that concentrations of 1%–5% NaOH improve the mechanical properties of composites made from various agricultural residues such as cotton stalks, wheat husks, and sugarcane bagasse [33–37].

Treatment of cotton stalks with a sodium hydroxide solution affected the chemical composition and caused a permanent decrease in the content of extractives, hemicellulose, and lignin, while the cellulose content of the cotton stalk particles increased steadily. Additionally, waxy and oil-based substances were effectively removed [34]. The wax layer on the surface of the straw contributed to water resistance, although also slightly reduced bonding strength. Removing the wax from the epidermis of rice straw via hexane extraction improved self-bonding [35], but sodium hydroxide treatment of cotton particle board, on the other hand, increased water absorption and thickness swelling [34].

The alkaline treatment of wheat husks with a 2% NaOH solution results in a cleaner husk surface, free of waxy substances and impurities. However, it also causes noticeable erosion of the husks, resulting in lower mechanical properties of composites made from the pretreated husks [38]. In tests of wheat straw-reinforced polyester resin, it was shown that treatment with a 2% sodium hydroxide solution leads to higher strength of the resulting composite [36]. Bartos et al. [37] investigated the optimal NaOH concentration for treating sugarcane bagasse fibers, finding that 5% NaOH provided the best tensile strength in polypropylene composites.

In the case of hydrophilic kenaf fibers, treatment with a 6% sodium hydroxide solution for 48 h improved compatibility with the polymer matrix and resulted in better mechanical properties in kenaf-epoxy composites [19]. Similarly, the effect of alkaline treatment on hemp fibers and their individual and interfacial properties in a polyurethane matrix has also been studied [39]. It was found that alkaline treatment enhances the mechanical properties of hemp fibers, with an 8% NaOH solution being identified as the upper limit for this improvement. This treatment effectively removed certain amounts of lignin and hemicellulose. Surface treatment of rape straw with sodium hydroxide has also been shown to improve adhesion between particles and adhesives [25,40].

The composition of rape straw is important in terms of the sorption of air moisture, as water molecules primarily bind to the amorphous regions of cellulose and hemicellulose [41–43]. However, surface treatment can also significantly influence moisture sorption. Previous studies have shown that treatment of rape straw with a 2% sodium hydroxide solution results in stronger adhesive bonding between the straw particles and the adhesive [22,44]. Despite this improvement, the treatment also had some negative effects, such as increased moisture absorption and consequent thickness swelling of the manufactured composite materials [38,40].

Moisture-related performance is particularly critical for building materials [45], as the moisture content (MC) of natural materials significantly affects both their mechanical and insulating properties [40,46–48]. Water sorption is also a key factor in the degradation of both straw [49] and composite building materials made from natural plant residues [50,51].

In this study, the surface of rape straw treated with 2% and 10% sodium hydroxide solutions was analyzed using SEM, EDS, FTIR, and XRD to investigate the structural and chemical changes induced by the alkaline treatment. These NaOH concentrations were chosen based on a review of the literature as the optimal and highest effective levels for straw modification. Following treatment, residual NaOH and leached products were observed on the straw surface, which are hypothesized to influence bonding processes in the production of eco-friendly composites from post-harvest residues. This research aimed to provide a detailed surface characterization of the treated straw, with a focus on identifying the particles formed. Additionally, as NaOH treatment may affect the straw's moisture sorption properties, the study also assessed the impact of these surface alterations on air moisture adsorption. Experimentally measured sorption isotherms were compared with generalized water vapor sorption models, contributing to a better

understanding of how treatment processes impact material performance in sustainable construction applications.

2 Materials and Methods

2.1 NaOH Treatment of Rape Straw

Straw from rapeseed grown in the village of Polepy near the Central Bohemian Highlands (Czech Republic) was used for the research. The reference straw was first washed with cold water to remove impurities from the surface. The maximum length of the straw was 120 mm, and the maximum diameter was 8–9 mm. This is the same straw that was used in our previous work [40]. Deionized water and sodium hydroxide (Kittfort Praha, Czech Republic; 99.5% NaOH) were used to prepare the sodium hydroxide solution. In this paper, the surface of rape straw was treated by soaking in 2% and 10% sodium hydroxide solution at a laboratory temperature of 23°C for 45 min. After both treatments, the sodium hydroxide solution was poured off. The rape straw samples were subsequently dried in an oven at 40°C.

2.2 Characterization of Rape Straw Surface Using SEM

The microstructural morphology of the rape straw surface was studied by scanning electron microscopy (SEM), using a Merlin-Zeiss field emission gun scanning electron microscope (FEG-SEM, Zeiss, Jena, Germany) with a secondary electron detector operated at an acceleration voltage of 5–15 kV, a probe current of 300–800 pA, and a working distance of 5–20 mm. The chemical composition of the treated and untreated rape straw surface was determined by energy-dispersive X-ray spectroscopy (EDS) using a Phenom XL desktop SEM (Thermo Fisher Scientific, Brno, Czech Republic) with an EDS detector operated at an acceleration voltage of 15 kV, and a working distance of 4–6 mm. All the samples for microscopic analysis were vacuum dried at room temperature. Using double-sided conductive carbon tape, vacuum-dried samples were then glued to an aluminum stab. Sputter coater Quorum SC7620 (Quorum Technologies Ltd., Laughton, United Kingdom) was used to generate an approximately 5–10 nm gold/palladium coating on the samples for the higher magnification by FEG-SEM and less than 5 nm of gold coating for elemental analysis via desktop SEM and magnification up to 2000×.

2.3 X-Ray Diffraction Analysis (XRD)

The X-ray diffractograms of material collected from the straw surface were acquired using a PANalytical Aeris diffractometer (Malvern PANalytical, Worcestershire, United Kingdom) equipped with CoK α tube operating at 40 kV and 7.5 mA. The incident beam path consisted of beta-filter iron, Soller slits 0.04 rad, and a divergence slit of 1/2°. The diffracted beam path was equipped with a 9 mm anti-scatter slit and Soller slits 0.04 rad. The detector used was a PIXcel1D-Medipix3 detector with an active length of 5.542°. The scan ranged from 5 to 75° 2 θ , step size 0.027°, and counting time 2.0325 s. Data were evaluated using Profex software (ver. 4.1.0, Nicola Döbelin, Solothurn, Switzerland) [52].

2.4 Determination of pH

To determine the pH of rape straw leachates, 100 g of straw per 1000 mL of distilled water was used. The samples were shaken on a REAX shaker for 24 h. The pH of each leachate was measured 5 times (in a volume of approximately 50 mL) by means of a PC70 portable multimeter (XS Instruments, Carpi, Italy; accuracy 0.01 pH).

2.5 Analysis of Leachates

The leakage of calcium and sodium from treated straw into the water was carried out using an Agilent 5110 (ICP-OES) inductively coupled plasma optical emission spectrometer (Agilent Technologies, Santa Clara, CA, USA) with synchronous vertical dual view and equipped with a SeaSpray concentric

nebulizer. The ICP-OES settings were as follows: radiofrequency power 1.2 kW; peristaltic pump speed 12 rpm; stabilization time 15 s; replicate read time 5 s; nebulizer flow $0.7 \text{ L}\cdot\text{min}^{-1}$; plasma flow $12 \text{ L}\cdot\text{min}^{-1}$; auxiliary argon flow $1 \text{ L}\cdot\text{min}^{-1}$. Ten replicates of each analyte were measured. An autosampler SPS 4 (Agilent Technologies, Santa Clara, CA, USA) was used for sample dosing, and pure argon (99.996 %, Linde Gas, Prague, Czech Republic) for measurement. Standard calcium solutions (Analytika, Prague, Czech Republic, $100 \text{ mg}\cdot\text{L}^{-1}$) were in the range of $1\text{--}100 \text{ mg}\cdot\text{L}^{-1}$. For sodium, the standard solutions ranged from $1 \text{ mg}\cdot\text{L}^{-1}$ to $10 \text{ g}\cdot\text{L}^{-1}$ (Analytika, Prague, Czech Republic). All standards were diluted with ultrapure demineralized water (resistivity at $25^\circ\text{C} \geq 18 \text{ M}\Omega \text{ cm}$). In order to select the optimal analytical wavelengths, both elements were measured at all available wavelengths. Subsequently, a wavelength was selected for concentration determination where no potential spectral interferences were present, and a low relative standard deviation (%RSD) was achieved. The wavelength of 317.933 nm was selected for the determination of calcium concentration. In the case of sodium, the appropriate wavelengths varied significantly depending on the intensity. For lower sodium concentrations, the wavelength used was 589.592 nm and for higher concentrations, the most suitable wavelengths were 568.263 nm and 330.298 nm . ICP Expert Software ver. 7.4 (Agilent Technologies, Santa Clara, CA, USA) was used for the evaluation.

2.6 Fourier-Transform Infrared Spectroscopy (FTIR)

The changes in the chemical structure caused by exposure to two different concentrations of sodium hydroxide were observed by FTIR spectroscopy. Spectra were obtained using a Nicolet 6700 Fourier transform infrared spectrometer (Thermo Fisher Scientific, Waltham, MA, USA) equipped with a reflective attachment in the ATR sampler using a diamond crystal. This arrangement allows for precise qualitative analysis without sample preparation. The measuring conditions were as follows: a spectral resolution of 4 cm^{-1} , 32 scans of each analysis, and a spectral wavenumbers range between 4000 and 400 cm^{-1} . Deconvolution of the bands, fitting with a Gaussian function, in the IR spectra was performed using OMNIC Software (ver. 8.3.103, Thermo Fisher Scientific, Waltham, MA, USA).

2.7 Water Vapor Adsorption Isotherms

The oven-dried samples of rape straw were placed in glass weighing dishes which were placed in the air-conditioning chamber (Climacell, BMT, Monroe, WA, USA; humidity range 10%–98% RH). Ten different samples were used for the reference straw and each treatment method. In the first humidity level, the relative humidity was set at 20% and 23°C . The weight of each sample was recorded until a constant mass was reached. A constant mass was reached when the results of two successive weighing operations, carried out at an interval of 24 h, did not differ more than 0.1 % from the mass of the test sample. The relative humidity in the conditioning chamber was then increased to 40%, 60%, 80%, 90%, and 98% RH. MS Excel 2016 (Microsoft Corporation, Redmond, WA, USA) was used for data recording and basic calculations. Fixed nonlinear regression in Statistica 13.3 Academic software (TIBCO, Santa Clara, CA, USA) was used to calculate the experimental model for sorption isotherms.

3 Results and Discussion

3.1 Microscopic Characterization of Rape Straw Surface

After treatment with the hydroxide solution, white crystallized minerals were visible on the surface of the rape straw. This mineralized surface was more evident on the outside of the larger particles, particularly after treatment with a 10% hydroxide solution, where the crystallized minerals formed visible clusters in some cases (see Fig. 1).

The differences between the surface of treated and untreated rape straw can be seen very clearly even at low magnification from the SEM images (Fig. 2).

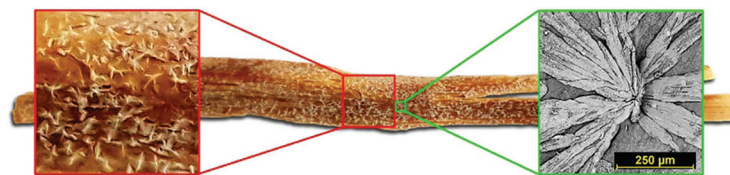


Figure 1: Example of straw treated with 10% hydroxide solution. The color section shows a macro image of the surface (Canon EOS 30D camera with a macro lens), and the black and white section shows an SEM image

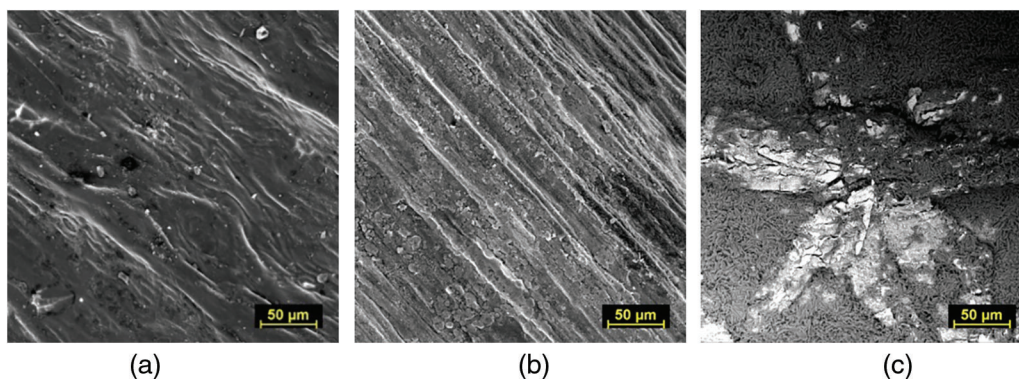


Figure 2: Surface images at 500 \times magnification of reference rape straw washed with water (a), treated with 2% NaOH solution (b), and 10% NaOH solution (c)

The surface of the water-washed rape straw is smooth, but despite thorough washing, it still contains small impurities. Small mineral crystals formed on the surface of rape straw treated with a 2% NaOH solution. On straws treated with a 10% NaOH solution, these crystals cluster and sometimes form star-like shapes. Figs. 3 and 4 show the straw surface after both treatment methods at a higher magnification.

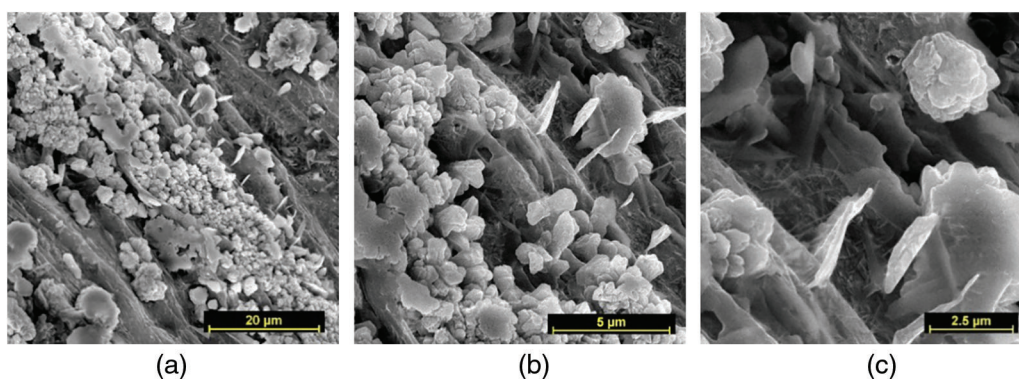


Figure 3: Microscopic images of rape straw treated with 2% NaOH solution at 2500 \times (a), 5000 \times (b), and 10,000 \times magnification (c)

Due to the processing technology and the size of the rape straw particles, the surface of the straw was often crushed during mixing. Nevertheless, it was possible to observe the crystalline nature of the treatment precipitates on the surface of the straw. At higher magnification (Fig. 3c), it can be seen that the fibers were also detached from the straw surface, although to a much lesser extent than during the 10% NaOH treatment.

When a 10% NaOH solution was used to treat rape straw, aggregation of leaching products occurred (Fig. 4a) and the surface of the straw particles was more disturbed (Fig. 4b,c).

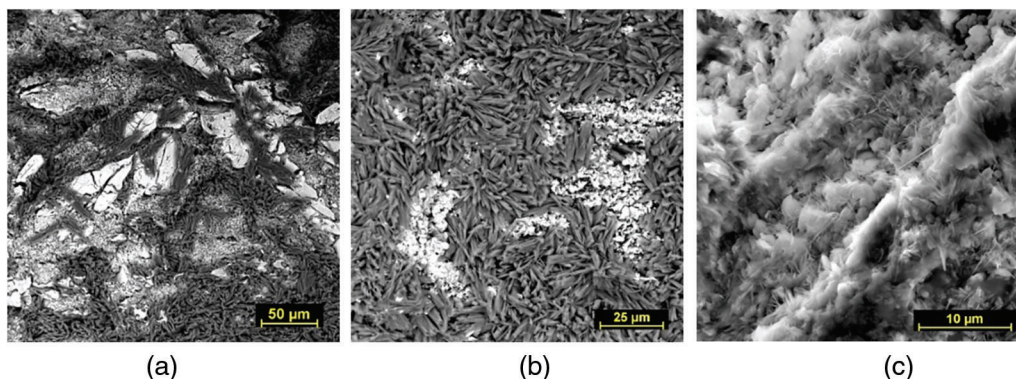


Figure 4: Microscopic images of rape straw treated with 10% NaOH solution at 1000× (a), 2000× (b), and 5000× magnification (c)

3.2 EDS Analysis of Rape Straw Surface

The results of the EDS analysis at 2000× magnification are shown in Fig. 5 (treatment with 2% NaOH solution) and Fig. 6 (treatment with 10% NaOH solution).

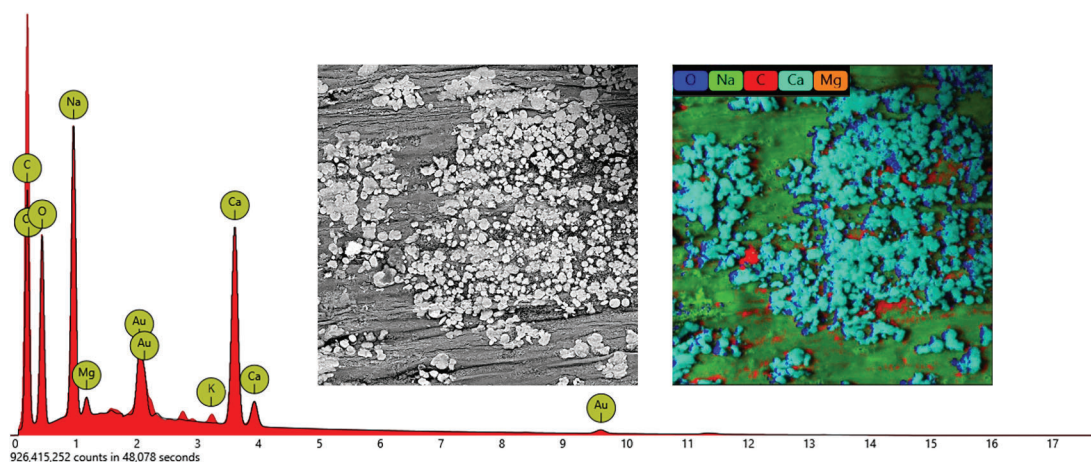


Figure 5: EDS spectrum and elemental map of rape straw treated with 2% NaOH solution. The displayed map has dimensions of 134 μm \times 134 μm and a resolution of 1024 px \times 1024 px

Using EDS analysis, the following elements were detected on the surface of rape straw in particular: O, Na, C, and Ca, whilst Mg could be found in smaller amounts, ranging between 0.5 and 1.5 wt%. Other elements such as K and Si appeared in some maps, but their amounts were usually below 1 wt%. The gold comes from the sputter-coated conductive layer. For clarity, these elements were not included in the elemental map. The hydrogen atoms are not detectable by the EDS.

From the elemental map, it can be seen that C and Ca predominate in places where the “treatment products” are found. Calcium also comes from rape straw, which contains several grams of calcium per kilogram of straw [25]. On the rest of the surface of the rape straw, Na is detected as the prevailing element.

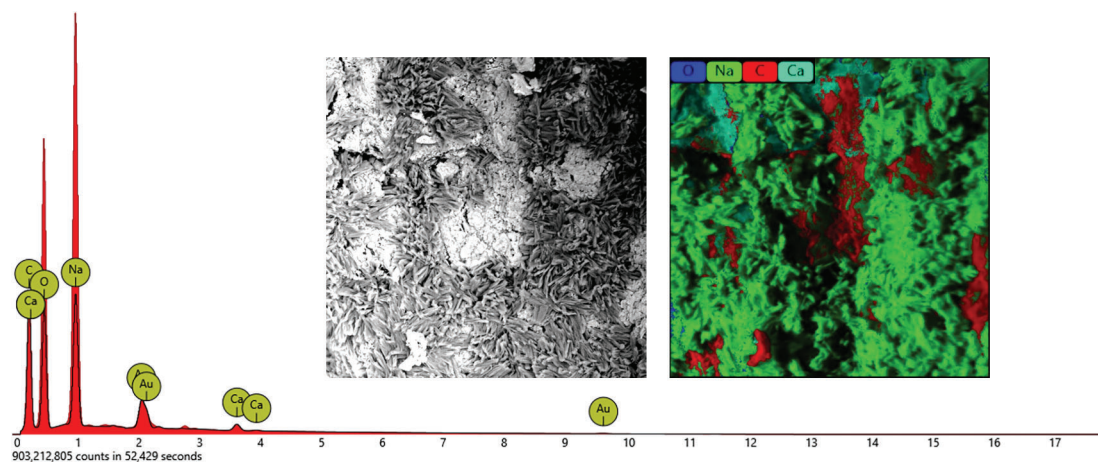


Figure 6: EDS spectrum and elemental map of rape straw treated with 10% NaOH solution. The displayed map has dimensions of $134\ \mu\text{m} \times 134\ \mu\text{m}$ and a resolution of $1024\ \text{px} \times 1024\ \text{px}$

After treatment of rape straw with 10% NaOH solution, the distribution of elements on its surface was similar, although the proportion of sodium increased even more (in this particular case from about 27 to 38 wt%).

3.3 XRD Results

The obtained powder X-ray diffractograms of individual samples are presented in Figs. 7–9.

The diffractogram collected from the rape straw before the alkaline treatment corresponded to the amorphous cellulose [53]. Only a small peak attributed to kaolinite was found, coming from the soil that clung to the straw.

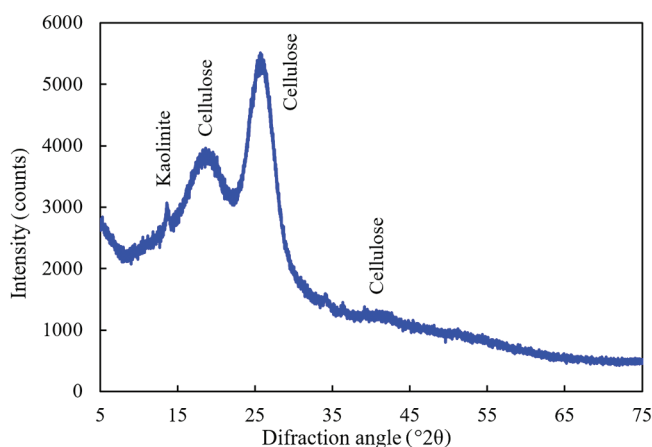


Figure 7: X-ray diffractogram of material scraped off the surface of untreated rape straw

The treatment of straw with 2% NaOH solution caused the precipitation of calcite (CaCO_3) crystals on the straw surface. The treatment with 10% NaOH likely also provided a small amount of calcite, but the straw surface was mainly covered by gaylussite $\text{Na}_2\text{Ca}(\text{CO}_3)_2 \cdot 5\text{H}_2\text{O}$ and thermonatrite $\text{Na}_2\text{CO}_3 \cdot \text{H}_2\text{O}$ crystals. The amorphous cellulose once again created a background in the diffractogram. The ratio of crystalline phases may be estimated roughly as 1:1 since the non-standard shape of the sample does not allow for precise quantification.

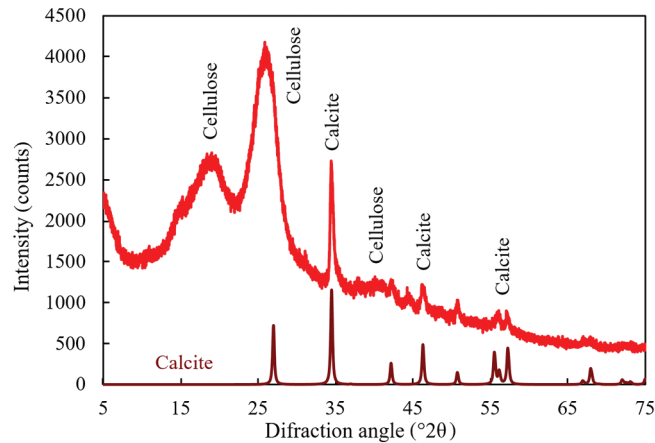


Figure 8: X-ray diffractogram of material scraped off the surface of rape straw treated with 2% NaOH

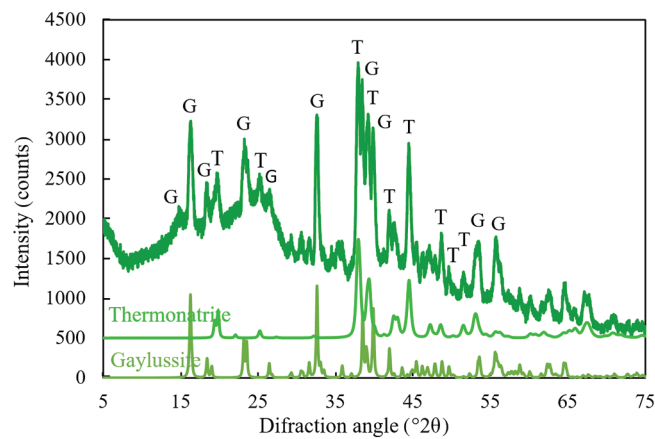


Figure 9: X-ray diffractogram of material scraped off the surface of rape straw treated with 10% NaOH. G–gaylussite $\text{Na}_2\text{Ca}(\text{CO}_3)_2 \cdot 5\text{H}_2\text{O}$; T–thermonatrite $\text{Na}_2\text{CO}_3 \cdot \text{H}_2\text{O}$

3.4 Sorption Isotherms

The water vapor sorption isotherms (Fig. 10) indicate that the NaOH treatment of rape straw significantly promoted the vapor sorption ability. The results of untreated rape straw were consistent with those of other lignocellulosic materials. At 98% relative humidity, the untreated rape straw showed a moisture content of $0.4 \text{ kg}\cdot\text{kg}^{-1}$, which was similar to that of wheat and rice straws published by Yin et al. [49]. Similar sorption isotherm values for untreated wheat straw were obtained by Han [54]. Hemp powder also showed the same isotherm curve at 20°C [55]. Slightly lower sorption was recorded for raw and also modified flax fiber [56]. Jute showed higher moisture content at 98% relative humidity of $0.38 \text{ kg}\cdot\text{kg}^{-1}$, while other lignocellulosic thermal insulation materials (wood fiber, flax, and hemp fiber) showed slightly lower water vapor storage parameters [57]. Alkali-treated rape straw exhibited significantly higher sorption in a whole range of relative humidity. Samples treated with 10% sodium hydroxide solution reached even higher values.

Based on the experimentally measured values, a model was calculated that best describes the fit of the sorption isotherms for rape straw treated with sodium hydroxide solutions. The suitability of the fit of this model was assessed using the coefficient of determination (R^2). This model of sorption isotherms differs from other lignocellulosic materials. The literature [58–60] suggested that for most natural hygroscopic

polymers, a curve with a sigmoidal shape is the most appropriate in order to describe moisture uptake. Calculations based on the Brunauer-Emmett-Teller theory (BET), the Dent model [59], and the Guggenheim-Anderson-de Boer model (GAB) [61] are most commonly used for moisture adsorption in cellulose. These models assume that the adsorbed moisture is bound both directly by hydrogen bridges of hydroxyl groups and by forces with lower binding energy (e.g., van der Waals forces) and are based on several different parameters. These models would be best fitted by a cubic polynomial model from the measured data. However, for the calculated cubic polynomial model, the coefficients of determination were in the range of 0.80–0.85. For the exponential model, R^2 values were higher in the range of 0.95–0.99 (Table 2). This different trend in moisture sorption implies the possible impact of mineral particles on the surface of the treated rape straw.

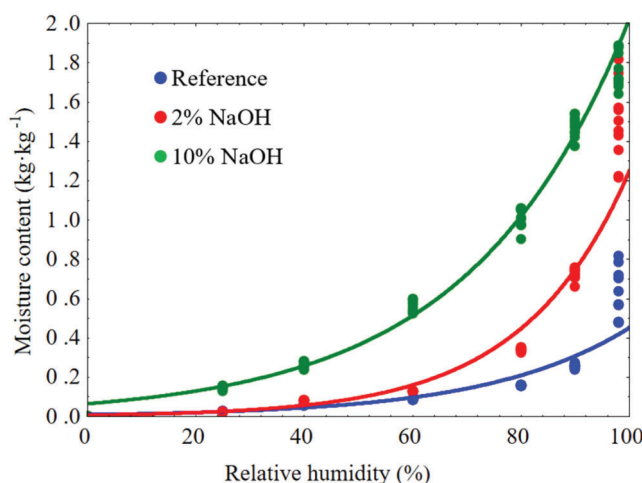


Figure 10: Sorption isotherms of untreated and alkali-treated rape straw

Table 2: Calculated sorption isotherms based on measured data

	Calculated sorption isotherms	R^2
Reference	$MC = 0.0098 \cdot \exp(0.0384 \cdot RH)$	0.988
2% NaOH	$MC = 0.0074 \cdot \exp(0.0513 \cdot RH)$	0.948
10% NaOH	$MC = 0.0657 \cdot \exp(0.0343 \cdot RH)$	0.950

Note: MC = Moisture content ($\text{kg} \cdot \text{kg}^{-1}$), RH = Relative humidity (%).

3.5 Applicability of Generalized Water Vapor Sorption Models

The sorption data obtained through experiments were analyzed so as to obtain more information about the process. For the calculation of the generalized model, the relative humidity was expressed in the form of relative pressure p_r , i.e., in the range of 0–1. The BET sorption isotherm (Eq. (1)) is a standard in materials research. Here, the a means the adsorbed amount of water ($\text{kg} \cdot \text{kg}^{-1}$), a_m denotes (in the original derivation of the BET model) the adsorbed amount needed for the entire sorbent surface to be covered by a monomolecular layer of sorbate (here it is water), and C is a dimensionless constant having relevance to the thermodynamics of the given sorption process. The unknown parameters a_m and C were obtained by plotting the experimental data in the linearized form of the BET isotherm (Eq. (2)), the linear part (slope and intercept) of which enables a simple calculation of the BET isotherm parameters (Table 3). The modeled isotherms were

compared with the experimental data (Fig. 11). It was observed that the BET isotherm is not able to describe the sorption behavior at high relative pressures.

$$a = a_m \frac{C \cdot p_r}{(1 - p_r) \cdot [1 + (C - 1) \cdot p_r]} \quad (1)$$

$$\frac{p_r}{a \cdot (1 - p_r)} = \frac{1}{a_m \cdot C} + \frac{C - 1}{a_m \cdot C} \cdot p_r \quad (2)$$

Table 3: Parameters of BET sorption isotherms

	C (-)	a_m ($\text{kg} \cdot \text{kg}^{-1}$)
Reference	5	0.036
2% NaOH	2	0.075
10% NaOH	3	0.690

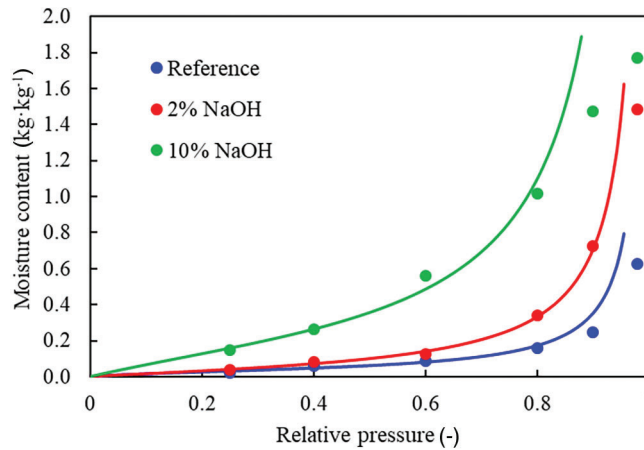


Figure 11: BET sorption isotherms

Given that the BET model was not providing a satisfactory fit with the experimental data, we searched for a better model. The Halsey, Henderson, and Lewicki models were tested but the most satisfying results were obtained by the GAB model [62] (Eq. (3)). This model was developed from BET assuming, among others, the effect of sorbate condensation [63]. The parameter m is again the adsorbed amount in the monolayer, F is the kinetic constant for sorption of the first layer, and G is the kinetic constant for multilayer sorption. The calculated isotherms (Table 4, Fig. 12) indicate the expected ability of this model to also properly describe the area of high relative pressure where moisture condensation takes place.

$$a = \frac{m \cdot F \cdot G \cdot p_r}{(1 - G \cdot p_r)(1 - G \cdot p_r + F \cdot G \cdot p_r)} \quad (3)$$

Both models, BET and GAB, determine the monolayer sorption capacity. In both cases, this value increases from untreated straw to a “10% NaOH” sample. Nevertheless, the absolute values of a_m (BET)

and m (GAB) are very different from each other. The GAB model is better at describing the sorption (including condensation), but that does not mean that the m values are physically correct for all the samples. The NaOH-treated samples are partially covered by treatment precipitates, thus there are two highly different types of surfaces (straw and mineral particles) and each of them will have its own “monolayer capacity.” The value acquired by models is just the “average” of two physically different systems (sorption on straw and sorption on minerals). The thermodynamic parameter C (BET) reached very different values as well, which again suggests a different sorption mechanism. The values of kinetic constant F (GAB, sorption of first layer) of “reference” and “2% NaOH” is nearly the same, while that of “10% NaOH” is much higher, thus implying the important effect of mineral particles, which are also responsible for very high sorption moisture content achieved by this sample in the full range of relative humidity. Finally, the G constant (GAB, multilayer sorption) is relatively similar for all samples.

Table 4: Parameters of GAB sorption isotherms

	m ($\text{kg}\cdot\text{kg}^{-1}$)	F (-)	G (-)
Reference	0.130	0.17	0.90
2% NaOH	0.332	0.22	0.88
10% NaOH	0.538	1.30	0.78

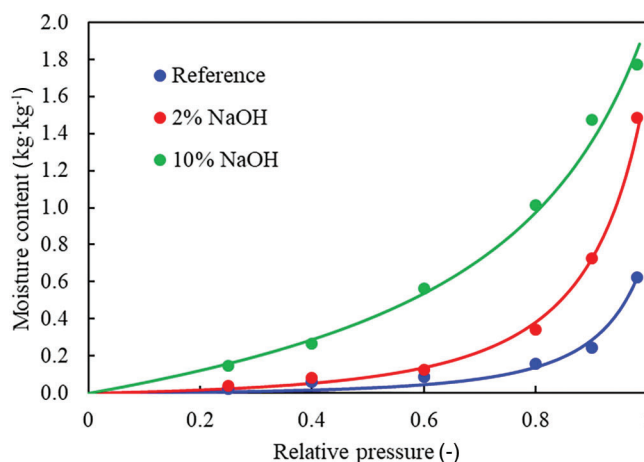


Figure 12: GAB sorption isotherms

3.6 Influence of Participating Mineral Particles

The first of the identified minerals—thermonatrite— $\text{Na}_2\text{CO}_3 \cdot \text{H}_2\text{O}$, is part of the hygroscopic reversible cycle described by (Eq. (4)) [64]. The humidification (water sorption, deliquescence) of anhydrous Na_2CO_3 starts at 60% RH, while the sodium carbonate solution is formed at 75% RH. There is a certain hysteresis loop, meaning that the dehydration of thermonatrite to anhydrous Na_2CO_3 does not take place until the RH drops to about 40%.



The second mineral, gaylussite, also contains crystalline water, but its behavior in dependence on RH is not described in the literature, according to our knowledge. Nevertheless, it is known that gaylussite stability

is sensitive to moisture changes [65]. The gaylussite may be also dehydrated thermally [66] (Eq. (5)) directly to anhydrous double-carbonate.

It is interesting to note that a dihydrate $\text{Na}_2\text{Ca}(\text{CO}_3)_2 \cdot 2\text{H}_2\text{O}$ (pirssonite) also exists. Thus, gaylussite also possibly contributes to the water vapor sorption/desorption of the treated straw.



With regard to the experimental results, we therefore assume that the increase in the adsorption of air moisture of rape straw treated with sodium hydroxide is a consequence not only of the disturbance of the straw surface [67] and a higher number of binding possibilities for water molecules [68], but also that the participating mineral particles also contribute to the higher hygroscopicity compared to the untreated straw.

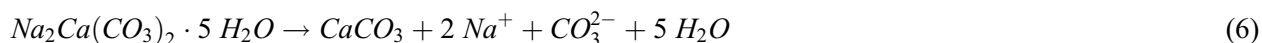
3.7 Determination of pH and Analysis of Leachates

The pH values of the water, sodium hydroxide solutions, and leachates obtained from the treated straw are summarized in Table 5.

Table 5: Average pH values and standard deviations

Sample	Mean pH	Std. Dev.
H ₂ O	7.13	0.067
2% NaOH	13.57	0.046
10% NaOH	13.52	0.061
Leachate-washed straw	6.49	0.040
Leachate-2% NaOH	11.97	0.031
Leachate-10% NaOH	13.31	0.071

The observed pH values for 2% and 10% sodium hydroxide solutions are obviously almost identical, but there are significant differences in the pH values of rape straw leachates treated with both solutions. The 2%-straw leachate reaches a pH of about 12. The only mineral identified here was calcite which is not soluble in water. Thus, the high pH of the leachate must be attributed to the dissolution of some of the residual NaOH from the straw surface. The pH of the 10%-straw leachate is significantly higher than the pH of the leachate after treatment with a 2% solution. This increase of pH is caused by the dissolution of thermonatrite (sodium carbonate). The second mineral—gaylussite—dissolves incongruently [69] into aragonite (a polymorph of CaCO_3) and soluble Na_2CO_3 , which again increases the pH of the solution (Eq. (6)).



The content of sodium and calcium in the treated rapeseed straw leachates was analyzed using ICP-OES. The results of the analysis are shown in Table 6.

Table 6: Concentration of selected elements in leachates from treated straw

Sample/element	Wavelength (nm)	Ca ($\text{mg}\cdot\text{L}^{-1}$)	Wavelength (nm)	Na ($\text{mg}\cdot\text{L}^{-1}$)
Leachate-washed straw	317.933	86.69 ± 0.45	589.592	16.11 ± 0.14
Leachate-2% NaOH	317.933	75.78 ± 0.49	568.263	4095 ± 19
Leachate-10% NaOH	317.933	56.65 ± 0.58	568.263	11270 ± 293

As can be seen from the table above, the concentration of calcium in the leachate does not change significantly after treatment with sodium hydroxide and remains approximately the same. Although microscopic analysis has shown that more calcium-containing mineral particles form on the surface of the straw with increasing NaOH concentration, calcium carbonate itself has a very low solubility in water and, therefore, has little effect on the amount of calcium in the leachate. Conversely, the treatment of straw with sodium hydroxide solution extensively increased the sodium ion content of the leachate compared to the untreated samples. The highest concentration of sodium in the leachate was found in the 10%-straw leachate, specifically $(11,270 \pm 293) \text{ mg}\cdot\text{L}^{-1}$, which is significantly different from the value of $(4095 \pm 19) \text{ mg}\cdot\text{L}^{-1}$ in the 2%-straw leachate and is several orders of magnitude higher than the leachate from untreated straw $(16.11 \pm 0.14) \text{ mg}\cdot\text{L}^{-1}$. Similar findings are reported in [70,71], also confirming that a substantial amount of sodium remains on the surface of straw after treatment with sodium hydroxide solution. Subsequently, after soaking, a significant proportion of the sodium ions are leached into the water [72].

3.8 Changes in the Chemical Structure of Straw after NaOH Treatment

Fig. 13 shows the infrared spectra recorded for three straw samples, namely the samples treated with 2% and 10% sodium hydroxide solution and the reference sample.

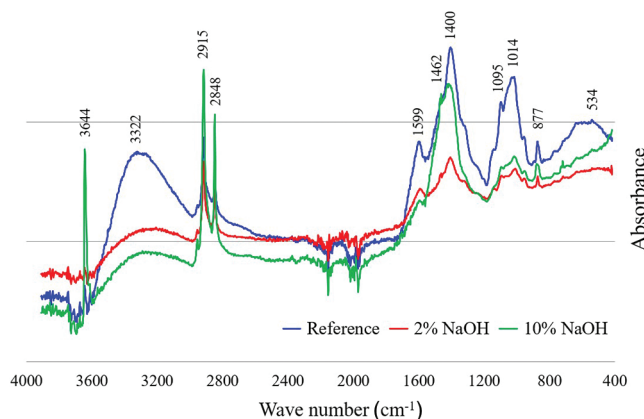


Figure 13: Infrared spectra of rape straw before and after NaOH treatment

All the samples analyzed can be characterized using the main absorption bands, the assignment of which is summarized in Table 7.

Table 7: Assignments of the major absorption bands

Wave numbers (cm^{-1})	Assignment
3644	stretching vibration (ν) of O-H in crystalline water molecules
3322	stretching vibration (ν) of O-H in water and saccharides
2915 and 2848	stretching antisymmetric (ν_{as}) and symmetric (ν_{s}) vibrations of C-H in $-\text{CH}_2-$ and $-\text{CH}_3$ aliphatic hydrocarbons
1599	bending vibration (δ) of C=C in an aromatic cycle and scissoring vibration (δ) of O-H in water

(Continued)

Table 7 (continued)	
Wave numbers (cm ⁻¹)	Assignment
1462	stretching vibration (ν) of C-O in carbonate anion
1400 and 877	stretching vibration (ν) of C=O in crystalline cellulose
1095	stretching vibration (ν) of C-O in saccharides
1014	stretching vibration (ν) of C-O-C in saccharides
below 600	deformation out-of-plane (γ) of C-O in saccharides

The first main region of the infrared spectra, 3700–3300 cm⁻¹, corresponds to the hydroxyl groups of the main components of the straw, such as cellulose, hemicellulose, and lignin molecules, as seen in the case of the reference sample. After treatment, more intense absorption bands can be observed at 3644 cm⁻¹ due to O-H bonds in crystalline water in the resulting mineral particles such as gaylussite, and thermonatrite, identified by XRD. The presence of residual NaOH clinging on the straw surface may also contribute to this absorption signal. On the other hand, the absorption band at 3322 cm⁻¹ decreases with increasing concentration of NaOH solution, indicating that the hydrogen bonds in the carbohydrates have been broken [73,74].

This trend is also visible at 1095 and 1014 cm⁻¹ for the absorption bands of C-O and C-O-C bonds in saccharides. The fundamental vibrations of C-H bonds in carbohydrates are demonstrated at 2915 and 2848 cm⁻¹, and carbonyl C=O bonds at 1400 cm⁻¹ as characteristic stretching and bending vibrations. The absorption band with a maximum at 1599 cm⁻¹ indicates aromatic C=C bonds in lignin [75] overlaps with the scissoring vibration of O-H in the crystalline cellulose at 1400 cm⁻¹ [76]. The absorption vibrations of C=O in the crystalline cellulose can be observed at 1400 and 877 cm⁻¹. At 877 cm⁻¹ the absorption band of C-C bonds vibration may occur, and thus the two opposing chemical processes contribute to the fact that the intensity of this band is almost identical for both the treated and reference samples. The wide absorption band below 600 cm⁻¹ can be assigned to the deformation out-of-plane vibrations of C-O-C bonds. The stretching vibration at 1462 cm⁻¹, apparent in the 10% NaOH sample, indicates the presence of carbonate anions.

As anticipated from the literature review, the experiments conducted, and the analysis of the results confirmed that the alkaline treatment removed some of the lignin and hemicellulose from the straw surface and also showed that mineral particles formed on the surface of the treated straw after treatment with sodium hydroxide solution.

3.9 Potential Further Uses of Alkaline-Modified Rape Straw

Low concentrations of sodium hydroxide are commonly used for the surface treatment of lignocellulosic particles for particleboard production; higher concentrations are rarely used. The use of higher concentrations of sodium hydroxide to treat the rape straw leads to greater surface disturbance and, in addition, mineral particles form on the surface which may further inhibit a stronger bond between the adhesive and the treated particles. Another possibility of using rape straw treated with sodium hydroxide solution is that the leached mineral particles will catalyze the bonding process. In a previous study [40], the formed mineral particles had a similar adhesive-enhancing effect on bone glue as lignosulfonate.

The minerals produced by treating straw with higher concentrations of sodium hydroxide may have other applications. Gaylussite is a sodium-calcium carbonate that is detected in some types of alkali-activated materials known as geopolymers. It was detected, for example, in alkali-activated blast furnace slag [77,78]. The occurrence of gaylussite on the surface of the straw can lead to ensuring compatibility

between the geopolymer gel and the straw. Geopolymers reinforced with surface-treated straw can then acquire better mechanical properties [79]. Similarly, treated straw could have a positive effect on cement hydration and mechanical properties of concrete [80,81].

The different moisture sorption characteristics of alkaline-treated straw also affect other parameters of composite materials. For instance, if insulation material for construction is produced from treated straw or similar post-harvest residues, the alkaline treatment will lead to changes in their thermal and hygroscopic properties. However, this assumption needs to be verified in future research.

4 Conclusions

This research analyzed the effect of alkaline treatment of rape straw surface on water vapor adsorption characteristics of straw. The novelty of the research lies in the identification of the mineral particles formed on the surface of the rape straw after treatment with sodium hydroxide and in the detailed description of their contribution to the sorption of air moisture of the treated rape straw. The main results can be summarized as follows:

- Surface disruption was found after the treatment of rape straw with sodium hydroxide solution, which increased with concentration.
- As the concentration of sodium hydroxide increased, the amount of sodium adhering to the straw surface also increased.
- After the treatment with sodium hydroxide, mineral particles were formed on the surface of the rape straw. For a 2% sodium hydroxide solution, calcite was primarily found on the surface of the straw. The use of a 10% sodium hydroxide solution resulted in the formation of gaylussite and thermonatrite.
- The mineral particles on the surface of the rape straw contributed to the adsorption of water vapor from the air. The equilibrium moisture content of treated rape straw was thus significantly higher than that of untreated straw over the whole RH range of 0% to 98% and increased with the concentration.
- The Guggenheim-Anderson-de Boer model was found to provide a very good fit to the measured adsorption isotherms, which corresponded well to the observed changes on the rape straw surface after the alkaline treatment.

Acknowledgement: The authors acknowledge the Czech Science Foundation for the financial support of this research.

Funding Statement: This research was supported by the Czech Science Foundation, under project No. 20-12166S.

Author Contributions: Martin Böhm: Conceptualization, Methodology, Investigation, Writing—original draft, Writing—review & editing. Miloš Jerman: Conceptualization, Investigation, Writing—original draft, Funding acquisition. Martin Keppert: Investigation, Formal analysis, Writing—review & editing. Klára Kobetičová: Investigation, Data curation, Validation. Dana Koňáková: Investigation, Formal analysis, Writing—original draft. Milena Pavlíková: Investigation, Formal analysis, Writing—original draft. Robert Černý: Supervision, Writing—review and editing. All authors reviewed the results and approved the final version of the manuscript.

Availability of Data and Materials: The datasets used are available upon request from the corresponding author.

Ethics Approval: Not applicable. The study involves only technical data and does not include human or animal subjects.

Conflicts of Interest: The authors declare no conflicts of interest to report regarding the present study.

References

1. Viel M, Collet F, Lanos C. Chemical and multi-physical characterization of agro-resources' by-product as a possible raw building material. *Ind Crops Prod.* 2018;120:214–37. doi:10.1016/j.indcrop.2018.04.025.
2. Cabrera FC. Eco-friendly polymer composites: a review of suitable methods for waste management. *Polym Compos.* 2021;42:2653–77. doi:10.1002/pc.26033.
3. Das O, Babu K, Shanmugam V, Sykam K, Tebyetekerwa M, Neisiany RE, et al. Natural and industrial wastes for sustainable and renewable polymer composites. *Renew Sustain Energy Rev.* 2022;158:1–22. doi:10.1016/j.rser.2021.112054.
4. United States Department of Agriculture (USDA). Oilseeds: world markets and trade. United States Department of Agriculture; 2024. Available from: <https://apps.fas.usda.gov/psdonline/circulars/oilseeds.pdf> [Accessed 2024].
5. Potůček F, Milichovský M. Rapeseed straw as a possible source of non-wood fibre materials. *Cellul Chem Technol.* 2011;45:23–8.
6. Kang KE, Jeong GT, Park DH. Pretreatment of rapeseed straw by sodium hydroxide. *Bioprocess Biosyst Eng.* 2012;35:705–13. doi:10.1007/s00449-011-0650-8.
7. Gupta R, McRoberts R, Yu Z, Smith C, Sloan W, You S. Life cycle assessment of biodiesel production from rapeseed oil: influence of process parameters and scale. *Bioresour Technol.* 2022;360:127532. doi:10.1016/j.biortech.2022.127532.
8. Noonari AA, Shah AR, Mirjat NH, Anh T. Various pretreatments of canola straw with hydrogen peroxide, calcium hydroxide, silica, and *Pleurotus ostreatus* to improve methane yield through anaerobic co-digestion. *Biomass Conv Bioref.* 2022;13:12903–15. doi:10.1007/s13399-021-02226-x.
9. Sikora A, Gaff M, Hysek Š, Babiak M. The plasticity of composite material based on winter rapeseed as a function of selected factors. *Compos Struct.* 2018;202:783–92. doi:10.1016/j.compstruct.2018.04.019.
10. Pińkowska H, Wolak P. Hydrothermal decomposition of rapeseed straw in subcritical water. Proposal of three-step treatment. *Fuel.* 2013;113:340–6. doi:10.1016/j.fuel.2013.05.088.
11. Mirzaee N, Nikzad M, Battisti R, Araghi A. Isolation of cellulose nanofibers from rapeseed straw via chlorine-free purification method and its application as reinforcing agent in carboxymethyl cellulose-based films. *Int J Biol Macromol.* 2023;251:126405. doi:10.1016/j.ijbiomac.2023.126405.
12. Cosereanu C, Cerbu C. Rape/wood particleboard. *BioResources.* 2019;14:2903–18. doi:10.15376/biores.14.2.2903-2918.
13. Tofanica BM. Rapeseed—a valuable renewable bioresource. *Cellul Chem Technol.* 2019;53:837–49. doi:10.35812/CelluloseChemTechnol.2019.53.81.
14. López-Linares JC, Cara C, Moya M, Ruiz E, Castro E, Romero I. Fermentable sugar production from rapeseed straw by dilute phosphoric acid pretreatment. *Ind Crops Prod.* 2013;50:525–31. doi:10.1016/j.indcrop.2013.08.028.
15. Greenhalf CE, Nowakowski DJ, Bridgwater AV, Titiloye J, Yates N, Riche A, et al. Thermochemical characterisation of straws and high yielding perennial grasses. *Ind Crops Prod.* 2012;36:449–59. doi:10.1016/j.indcrop.2011.10.025.
16. Hýsek Š, Gaff M, Sikora A, Babiak M. New composite material based on winter rapeseed and his elasticity properties as a function of selected factors. *Compos Part B Eng.* 2018;153:108–16. doi:10.1016/j.compositesb.2018.07.042.
17. Deykun I, Halysh V, Barbash V. Rapeseed straw as an alternative for pulping and papermaking. *Cellul Chem Technol.* 2018;52:833–9.
18. Mohammad S, Mousavi M, Ziaeddin S, Resalati H, Mahdavi S, Rasooly E. Papermaking potential of rapeseed straw, a new agricultural-based fiber source. *J Clean Prod.* 2013;52:420–4. doi:10.1016/j.jclepro.2013.02.016.
19. Fiore V, Di Bella G, Valenza A. The effect of alkaline treatment on mechanical properties of kenaf fibers and their epoxy composites. *Compos Part B Eng.* 2015;68:14–21. doi:10.1016/j.compositesb.2014.08.025.

20. Singh AK, Bedi R, Khajuria A. A review of composite materials based on rice straw and future trends for sustainable composites. *J Clean Prod.* 2024;457:142417. doi:10.1016/j.jclepro.2024.142417.
21. Ma Y, Shen Y, Liu Y. State of the art of straw treatment technology: challenges and solutions forward. *Bioresour Technol.* 2020;313:123656. doi:10.1016/j.biortech.2020.123656.
22. Hýsek Š., Sikora A, Schönfelder O, Böhm M. Physical and mechanical properties of boards made from modified rapeseed straw particles. *BioResources.* 2018;13:6396–408. doi:10.15376/biores.13.3.6396-6408.
23. Hýsková P, Hýsek Š., Schönfelder O, Šedivka P, Lexa M, Jarský V. Utilization of agricultural rests: straw-based composite panels made from enzymatic modified wheat and rapeseed straw. *Ind Crops Prod.* 2020;144. doi:10.1016/j.indcrop.2019.112067.
24. Choi CH, Um BH, Kim YS, Oh KK. Improved enzyme efficiency of rapeseed straw through the two-stage fractionation process using sodium hydroxide and sulfuric acid. *Appl Energy.* 2013;102:640–6. doi:10.1016/j.apenergy.2012.08.011.
25. Částková T, Hýsek Š., Sikora A, Schönfelder O, Böhm M. Chemical and physical parameters of different modifications of rape straw (*Brassica napus* L.). *BioResources.* 2018;13:104–14.
26. Koohestani B, Darban AK, Mokhtari P, Yilmaz E, Darezereshki E. Comparison of different natural fiber treatments: a literature review. *Int J Environ Sci Technol.* 2019;16:629–42.
27. Brahim M, El Kantar S, Boussetta N, Grimi N, Brosse N, Vorobiev E. Delignification of rapeseed straw using innovative chemo-physical pretreatments. *Biomass Bioenergy.* 2016;95:92–8. doi:10.1016/j.biombioe.2016.09.019.
28. Firsty VG, Jeong JY, Gu YM, Lee JH, Shin SJ. High cellulose purity by acid hydrolysis pretreatment on kenaf outer bast. *Appl Sci.* 2023;13. doi:10.3390/app13010334.
29. Wu S, Shi S, Liu R, Wang C, Li J, Han L. The transformations of cellulose after concentrated sulfuric acid treatment and its impact on the enzymatic saccharification. *Biotechnol Biofuels Bioprod.* 2023;16:1–10. doi:10.1186/s13068-023-02293-4.
30. Suopajarvi T, Ricci P, Karvonen V, Ottolina G, Liimatainen H. Acidic and alkaline deep eutectic solvents in delignification and nanofibrillation of corn stalk, wheat straw, and rapeseed stem residues. *Ind Crops Prod.* 2020;145:111956. doi:10.1016/j.indcrop.2019.111956.
31. Bichi AH, Zhang K, Yang J, Chen D. Analysis of the properties of alkaline-treated rape straw and stalk polyvinyl chloride composites. *Text Res J.* 2022;92:4008–19. doi:10.1177/00405175221098586.
32. Renreng I, Bakri B, Chandrabakty S, Naharuddin. Evaluation of mechanical and physical properties of pressed coir fiber/epoxy composite with NaOH and microwave treatment of fiber. *J Renew Mater.* 2021;9:325–35. doi:10.32604/jrm.2021.012774.
33. Hýsek Š., Podlena M, Böhm M, Bartsch H. Effect of cold plasma surface pre-treatment of wheat straw particles on straw board properties. *BioResources.* 2018;13(3):5065–79. doi:10.15376/biores.13.3.5065-5079.
34. Yaşar S, İçel B. Alkali modification of cotton (*Gossypium hirsutum* L.) stalks and its effect on properties of produced particleboards. *BioResources.* 2016;11:7191–204. doi:10.15376/biores.11.3.7191-7204.
35. Chen W, Xu Y, Shi S, Cao Y, Chen M, Zhou X. Fast modification on wheat straw outer surface by water vapor plasma and its application on composite material. *Sci Rep.* 2018;8:4–11. doi:10.1038/s41598-018-20285-5.
36. Haque ME, Khan MW, Rani M. Studies on morphological, physico-chemical and mechanical properties of wheat straw reinforced polyester resin composite. *Polym Bull.* 2022;79:2933–52. doi:10.1007/s00289-021-03630-z.
37. Bartos A, Utomo BP, Kanyar B, Anggono J, Soetaredjo FE, Móczó J, et al. Reinforcement of polypropylene with alkali-treated sugarcane bagasse fibers: mechanism and consequences. *Compos Sci Technol.* 2020;200:108428. doi:10.1016/j.compscitech.2020.108428.
38. Hýsek Š., Podlena M, Bartsch H, Wenderdel C, Böhm M. Effect of wheat husk surface pre-treatment on the properties of husk-based composite materials. *Ind Crops Prod.* 2018;125:105–13. doi:10.1016/j.indcrop.2018.08.035.
39. Sair S, Oushabi A, Kammouni A, Tanane O, Abboud Y, Hassani FO, et al. Effect of surface modification on morphological, mechanical and thermal conductivity of hemp fiber: characterization of the interface of hemp-polyurethane composite. *Case Stud Therm Eng.* 2017;10:550–9. doi:10.1016/j.csite.2017.10.012.

40. Dušek J, Jerman M, Podlena M, Böhm M, Černý R. Sustainable composite material based on surface-modified rape straw and environment-friendly adhesive. *Constr Build Mater.* 2021;300:124036. doi:10.1016/j.conbuildmat.2021.124036.
41. Zografi G, Kontny MJ, Yang AYS, Brenner GS. Surface area and water vapor sorption of macrocrystalline cellulose. *Int J Pharm.* 1984;18:99–116. doi:10.1016/0378-5173(84)90111-X.
42. Fredriksson M, Rüggeberg M, Nord-Larsen T, Beck G, Thybring EE. Water sorption in wood cell walls-data exploration of the influential physicochemical characteristics. *Cellulose.* 2023;30:1857–71. doi:10.1007/s10570-022-04973-0.
43. Simon M, Fulchiron R, Gouanvé F. Water sorption and mechanical properties of cellulosic derivative fibers. *Polymers.* 2022;14:2836. doi:10.3390/polym14142836.
44. Gaff M, Hýsek Š., Sikora A, Babiak M. Newly developed boards made from crushed rapeseed stalk and their bendability properties. *BioResources.* 2019;13:4776–94. doi:10.15376/biores.13.3.4776-4794.
45. Nor Arman NS, Chen RS, Ahmad S. Review of state-of-the-art studies on the water absorption capacity of agricultural fiber-reinforced polymer composites for sustainable construction. *Constr Build Mater.* 2021;302:124174. doi:10.1016/j.conbuildmat.2021.124174.
46. Bachchan AA, Das PP, Chaudhary V. Effect of moisture absorption on the properties of natural fiber reinforced polymer composites: a review. *Mater Today: Proc.* 2020;49:3403–8. doi:10.1016/j.matpr.2021.02.812.
47. Jerman M, Böhm M, Dušek J, Černý R. Effect of steaming temperature on microstructure and mechanical, hygric, and thermal properties of binderless rape straw fiberboards. *Build Environ.* 2022;223:109474. doi:10.1016/j.buildenv.2022.109474.
48. Dukarska D, Czarnecki R, Dziurka D, Mirski R. Construction particleboards made from rapeseed straw glued with hybrid pMDI/PF resin. *Eur J Wood Wood Prod.* 2017;75:175–84. doi:10.1007/s00107-016-1143-x.
49. Yin X, Lawrence M, Maskell D, Ansell M. Comparative micro-structure and sorption isotherms of rice straw and wheat straw. *Energy Build.* 2018;173:11–8. doi:10.1016/j.enbuild.2018.04.033.
50. Elfaleh I, Abbassi F, Habibi M, Ahmad F, Guedri M, Nasri M, et al. A comprehensive review of natural fibers and their composites: an eco-friendly alternative to conventional materials. *Results Eng.* 2023;19:101271. doi:10.1016/j.rineng.2023.101271.
51. Mohammed M, Oleiwi JK, Mohammed AM, Jawad AJM, Osman AF, Adam T, et al. A review on the advancement of renewable natural fiber hybrid composites: prospects, challenges, and industrial applications. *J Renew Mater.* 2024;12:1237–90. doi:10.32604/jrm.2024.051201.
52. Doebelin N, Kleeberg R. Profex: a graphical user interface for the Rietveld refinement program BGMN. *J Appl Crystallogr.* 2015;48:1573–80. doi:10.1107/S1600576715014685.
53. Yu S, Liu Z, Xu N, Chen J, Gao Y. Influencing factors for determining the crystallinity of native cellulose by X-ray diffraction. *Anal Sci.* 2020;36:947–51. doi:10.2116/analsci.19P427.
54. Han G, Cheng W, Deng J, Dai C, Zhang S, Wu Q. Effect of pressurized steam treatment on selected properties of wheat straws. *Ind Crops Prod.* 2009;30:48–53. doi:10.1016/j.indcrop.2009.01.004.
55. Oduola AA, Luthra K, Atungulu GG. Determination of moisture sorption isotherms of industrial hemp (*Cannabis sativa* L.) flower and leaf composite powders. *Ind Crops Prod.* 2022;186:115201. doi:10.1016/j.indcrop.2022.115201.
56. Karoyo AH, Dehabadi L, Alabi W, Simonson CJ, Wilson LD. Hydration and sorption properties of raw and milled flax fibers. *ACS Omega.* 2020;5:6113–21. doi:10.1021/acsomega.0c00100.
57. Jerman M, Palomar I, Kočí V, Černý R. Thermal and hygric properties of biomaterials suitable for interior thermal insulation systems in historical and traditional buildings. *Build Environ.* 2019;154:81–8. doi:10.1016/j.buildenv.2019.03.020.
58. Limousin G, Gaudet JP, Charlet L, Szenknect S, Barthès V, Krimissa M. Sorption isotherms: a review on physical bases, modeling and measurement. *Appl Geochem.* 2007;22:249–75. doi:10.1016/j.apgeochem.2006.09.010.
59. Ouertani S, Azzouz S, Hassini L, Koubaa A, Belghith A. Moisture sorption isotherms and thermodynamic properties of Jack pine and palm wood: comparative study. *Ind Crops Prod.* 2014;56:200–10. doi:10.1016/j.indcrop.2014.03.004.

60. Hou S, Wang J, Yin F, Qi C, Mu J. Moisture sorption isotherms and hysteresis of cellulose, hemicelluloses and lignin isolated from birch wood and their effects on wood hygroscopicity. *Wood Sci Technol.* 2022;56:1087–102. doi:10.1007/s00226-022-01393-y.
61. Thybring EE, Boardman CR, Zelinka SL, Glass SV. Common sorption isotherm models are not physically valid for water in wood. *Colloids Surfaces A Physicochem Eng Asp.* 2021;627:127214. doi:10.1016/j.colsurfa.2021.127214.
62. Majd KM, Razavizadeh N, Karparvarfard SH. Study of moisture sorption thermodynamic in canola oilseed and drying energy requirement considerations. *J Food Process Eng.* 2024;47:1–12. doi:10.1111/jfpe.14743.
63. Jraba G, Salem N, Neji J. Effect of *Posidonia oceanica* on the hygrothermal characterization of compacted earth blocks. *Constr Build Mater.* 2024;411:134569. doi:10.1016/j.conbuildmat.2023.134569.
64. Pang S, Zhang Y, Ma S, Yang M. Hygroscopic growth and phase transitions of Na_2CO_3 and Mixed $\text{Na}_2\text{CO}_3/\text{Li}_2\text{CO}_3$ particles: influence of Li_2CO_3 on phase transitions of Na_2CO_3 and formation of LiNaCO_3 . *J Phys Chem A.* 2020;124:10870–78. doi:10.1021/acs.jpca.0c08891.
65. Johnson DR, Robb WA. Gaylussite: thermal properties by simultaneous thermal analysis. *Am Mineral.* 1973;58:778–84.
66. Royce K, Baars C. Caring for geological collections: unresolved questions. *J Nat Sci Collect.* 2021;8:28–38.
67. Rothenhäusler F, Ouali AA, Rinberg R, Demleitner M, Kroll L, Ruckdaeschel H. Influence of sodium hydroxide, silane, and siloxane treatments on the moisture sensitivity and mechanical properties of flax fiber composites. *Polym Compos.* 2024;45:8937–48. doi:10.1002/pc.28386.
68. Hýsek Š., Čermák J, Lexa M. Influence of lignocellulosic waste pre-treatment on the characteristics of bond rupture. *Sustainability.* 2019;11(17):4784. doi:10.3390/su11174784.
69. Bischoff JL, Herbst DB, Rosenbauer RJ. Gaylussite formation at Mono Lake, California. *Geochim Cosmochim Acta.* 1991;55:1743–7. doi:10.1016/0016-7037(91)90144-T.
70. Jackson MG. The alkali treatment of straws. *Anim Feed Sci Technol.* 1977;2:105–30. doi:10.1016/0377-8401(77)90013-X.
71. Sebestyén Z, May Z, Réczey K, Jakab E. The effect of alkaline pretreatment on the thermal decomposition of hemp. *J Therm Anal Calorim.* 2011;105:1061–9. doi:10.1007/s10973-010-1056-6.
72. Boonterm M, Sunyadeth S, Dedpakdee S, Athichalinthorn P, Patcharaphun S, Mungkung R, et al. Characterization and comparison of cellulose fiber extraction from rice straw by chemical treatment and thermal steam explosion. *J Clean Prod.* 2016;134:592–9. doi:10.1016/j.jclepro.2015.09.084.
73. Dong L, Cao G, Wu J, Liu B, Xing D, Zhao L, et al. High-solid pretreatment of rice straw at cold temperature using NaOH/Urea for enhanced enzymatic conversion and hydrogen production. *Bioresour Technol.* 2019;287:121399. doi:10.1016/j.biortech.2019.121399.
74. Huang Y, Yin Z, Liu M, Li M, Zuo Y, Qing Y, et al. Effect of multi-hydroxyl polymer-treated MUF resin on the mechanical properties of particleboard manufactured with reed straw. *J Renew Mater.* 2023;11:3417–31. doi:10.32604/jrm.2023.028511.
75. Emmanuel V, Odile B, Céline R. FTIR spectroscopy of woods: a new approach to study the weathering of the carving face of a sculpture. *Spectrochim Acta—Part A Mol Biomol Spectrosc.* 2015;136:1255–9. doi:10.1016/j.saa.2014.10.011.
76. Dar MA, Syed R, Pawar KD, Dhole NP, Xie R, Pandit RS, et al. Evaluation and characterization of the cellulolytic bacterium, *Bacillus pumilus* SL8 isolated from the gut of oriental leafworm *Spodoptera litura*: an assessment of its potential value for lignocellulose bioconversion. *Environ Technol Innov.* 2022;27:102459. doi:10.1016/j.eti.2022.102459.
77. Marple MAT, Koroglu B, Morrison K, Crowhurst J, Balachandra A, Soroushian P, et al. Accelerated carbonation and structural transformation of blast furnace slag by mechanochemical alkali-activation. *Cem Concr Res.* 2022;156:106760. doi:10.1016/j.cemconres.2022.106760.
78. Kovtun M, Kearsley EP, Shekhovtsova J. Chemical acceleration of a neutral granulated blast-furnace slag activated by sodium carbonate. *Cem Concr Res.* 2015;72:1–9. doi:10.1016/j.cemconres.2015.02.014.

79. Maslyk M, Gäb T, Matveeva G, Opitz P, Mondeshki M, Krysiak Y, et al. Multistep crystallization pathways in the ambient-temperature synthesis of a new alkali-activated binder. *Adv Funct Mater.* 2022;32:2108126. doi:10.1002/adfm.202108126.
80. Bubeník J, Zach J, Křížová K, Novák V, Sedlmajer M, Žižková N. Behavior and properties of ultra-lightweight concrete with foamed glass aggregate and cellulose fibres under high temperature loading. *J Build Eng.* 2023;72:106677. doi:10.1016/j.jobbe.2023.106677.
81. Wen L, Yan C, Shi Y, Wang Z, Liu G, Shi W. Experimental study on the compressive strength of concrete with different wheat straw treatment techniques. *J Renew Mater.* 2023;11:3681–92. doi:10.32604/jrm.2023.027671.